

Prediction of the Elemental Content of Thin Films Electrodeposited from a Multi-component Solution: Co–Ni–Fe– Mn Thin Film as an Example of Multi-element Electrodeposits

M. Saitou

University of the Ryukyus, Department of Mechanical Systems Engineering, 1 Senbaru Nishihara-cho
Okinawa, 903-0213, Japan.

E-mail: saitou@tec.u-ryukyu.ac.jp

Received: 8 March 2020 / Accepted: 17 April 2020 / Published: 10 June 2020

The elemental content of Co–Ni–Fe–Mn thin films electrodeposited by a rectangular pulse voltage were investigated using energy dispersive X-ray microscopy (EDX). The EDX analyses revealed that the behaviors of the mean elemental content M_i , where i denotes an element of the Co–Ni–Fe–Mn thin films, were divided into three groups by the potential barrier V_{bi} and cathode potential V_c : (a) for $V_c > V_{bi}$, the values of M_i were consistent with the activity S_i of element- i in the solution, (b) for $V_c = V_{bi}$, the oscillation of the element- i content occurred at specific frequencies of the rectangular pulse voltage, and (c) for $V_c < V_{bi}$, M_i were determined by $S_i J_i$ where J_i denotes the current in the Fowler–Nordheim equation that represents the emission of electrons from the Fermi level to the energy level of i -ions on the electric double layer. This study demonstrated that the elemental contents of multi-element electrodeposits can be predicted using V_{bi} and V_c .

Keywords: Multi-component electrodeposit; Potential barrier; Cathode potential; Fowler–Nordheim equation;

1. INTRODUCTION

The prediction of the elemental content of multi-element thin films electrodeposited using a multi-component solution plays an important role in their applications in a variety of fields [1–2]. However, experimental studies have not focused on the relationship between the elemental content of electrodeposits and those in a multi-component solution. Currently, no phenomenological theory allows for the determination of the elemental content of multi-component electrodeposits formed from multi-component solutions [3]. For example, in the case of the use of the Butler–Volmer (BV) equation for two elements A and B: (1) when the BV equation for element A is larger than that for element B at any cathode potential, the molar ratio A/B of the A–B electrodeposit increases with the cathode potential,

(2) when the BV equation for element A intersects with that for element B, the molar ratio A/B indicates a constant only at the intersection point, but does not attain a constant independent of the cathode potential.

The energy band theory used in solid state physics [4] explains the electro-magnetic properties of solids. Electron emission from metal surfaces is described by the Fowler–Nordheim (FN) equation [5–7]. When metal surfaces to which a high electric field is applied have potential barriers, such as the work function, electrons are emitted through the potential barrier. This tunneling phenomenon of electrons obeys the FN equation. The electric double layer formed on the cathode is considered to play the same role as the potential barrier. Hence, The FN equation will allow us to describe the current through the electric double layer. Unlike the BV equation, the FN equation describes the contents of a multi-component electrodeposit. In this study, the quaternary Co–Ni–Fe–Mn alloy was chosen as a multi-component electrodeposit.

The aim of the present study is to demonstrate that the elemental content of the Co–Ni–Fe–Mn thin films can be predicted using the concepts of the cathode potential and the potential barrier, and the FN equation.

2. EXPERIMENTAL SETUP

A copper plate of $15 \times 10 \text{ mm}^2$ and a carbon plate of $50 \times 40 \text{ mm}^2$ were prepared for the cathode and anode. One side of the copper plate was electrically insulated to avoid the deposition of a Co–Ni–Fe–Mn thin film. An aqueous solution containing the following chemical compounds was used: 1.0 mol/L $\text{CoSO}_4 \cdot 7\text{H}_2\text{O}$, 2.7 mol/L $\text{NiSO}_4 \cdot 6\text{H}_2\text{O}$, 0.45 mol/L $\text{FeSO}_4 \cdot 7\text{H}_2\text{O}$, 0.45 mol/L $\text{MnSO}_4 \cdot 5\text{H}_2\text{O}$, and 0.65 mol/L $\text{KNaC}_4\text{H}_4\text{O}_6 \cdot 4\text{H}_2\text{O}$. The cathode and anode were placed parallel to each other in a cell filled with the aqueous solution maintained at 298 K during electrodeposition.

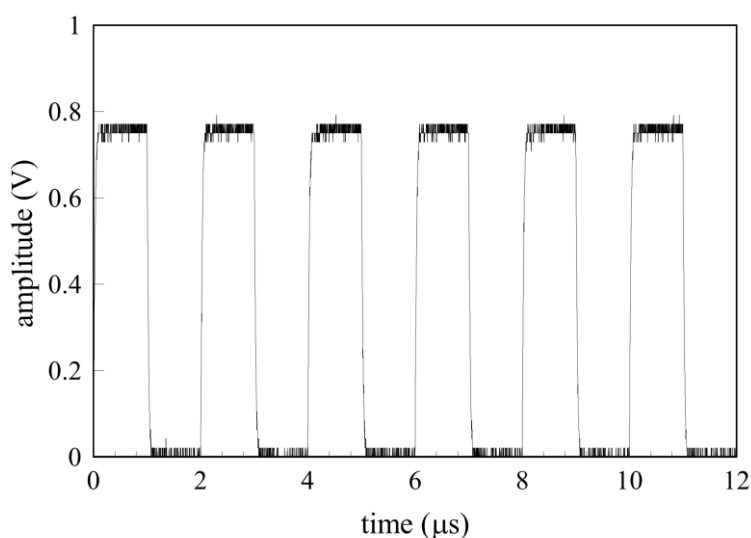


Figure 1. The rectangular pulse voltage measured across the 22Ω resistor corresponding to a 3.05 V rectangular pulse applied to the cell.

A rectangular pulse voltage in the range of 0.4–1.2 MHz was supplied to the cell by a function generator. A 22 Ω metal film resistor was connected in series with the cell to determine the current density flowing to the cell. The impedance of the metal film resistor was independent of the frequency under 80 MHz. Figure 1 shows typical voltage drops measured across the 22 Ω metal film resistor when a rectangular pulse voltage with an amplitude of 3.05 V and a frequency of 0.5 MHz was applied to the cell.

After electrodeposition, the Co–Ni–Fe–Mn thin films electrodeposited on the copper plate were rinsed with distilled water. The Co–Ni–Fe–Mn thin films were weighed to a precision of 0.1 mg with an electric balance to estimate the film thicknesses of the Co–Ni–Fe–Mn thin films. The elemental content of the Co–Ni–Fe–Mn thin films on the copper plate were investigated using energy dispersive X-ray spectroscopy (SEM–EDX: Hitachi TM3030).

3. RESULTS AND DISCUSSION

3.1. Energy band diagram of electrons in the Cu electrode and ions in the solution

Figure 2 (a) shows the energy band diagrams of electrons in the Cu electrode and i^{2+} ions in the solution when no rectangular pulse voltage was applied to the cell. When the Cu electrode was dipped in the solution, the Fermi energy level of the Cu electrode was consistent with the chemical potential of the solution, and attained the thermal equilibrium. The i^{2+} and ion i^+ ions have upper and lower state energy levels, respectively. The energy difference between the Fermi energy level and the upper energy level is called as the potential barrier. An electron at the Fermi energy level in the Cu electrode cannot transfer to the upper energy level of i^{2+} through the electric double layer, which acts as an insulator. Once the i^{2+} ion receives one electron, the formed i^+ ion can promptly receive one electron owing to its energy level [8] being lower than the Fermi energy level.

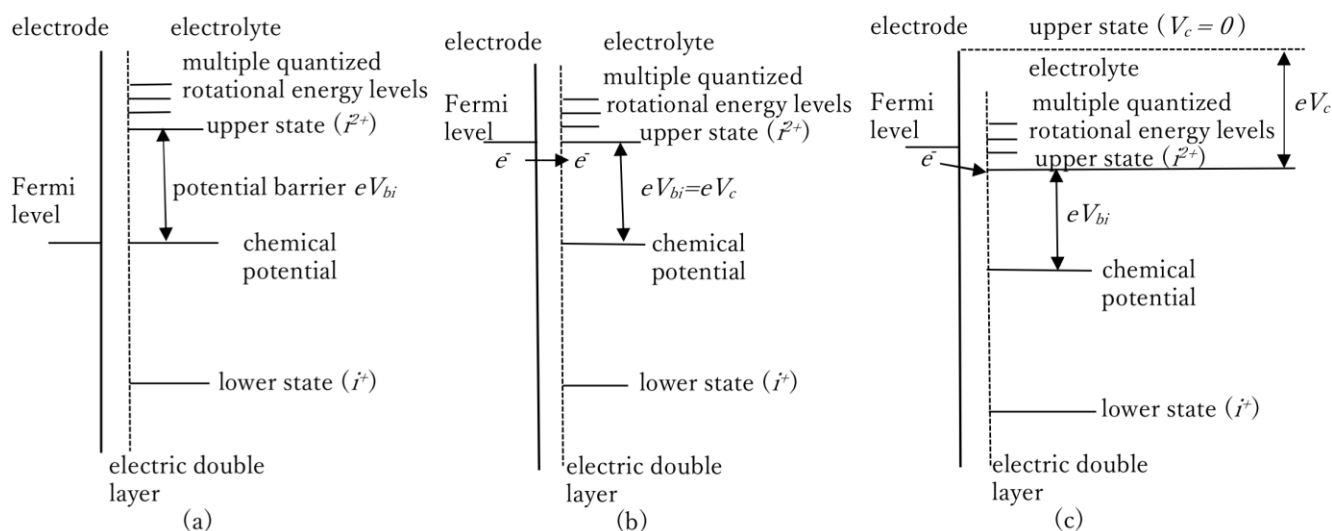


Figure 2. Energy band diagrams of the Cu cathode and ions in the solution: (a) $V_c = 0$, (b) $V_c = V_{bi}$, and (c) $V_c > V_{bi}$.

When the voltage applied to the cell allows the chemical potential to move below the Fermi energy level, the current flows through the cell gradually owing to the tunneling effect through the electric double layer, which acts as the insulator. This is because the thickness of the electric double layer is several angstroms. The tunneling current J is described by the FN equation [5]:

$$J \propto V^2 \exp\left(-\alpha \frac{\phi^{3/2}}{F}\right), \quad (1)$$

where V is the voltage applied to the electric double layer, F defined by $F = \beta V$ where β is the field amplification factor, is the strength of the electric field, ϕ is the work function, and α is $6.83 \times 10^7 \text{ V}^{-1/2} \text{ cm}^{-1}$. Equation (1) can be rewritten as

$$\ln\left(\frac{J}{V^2}\right) \propto -\alpha \frac{\phi^{3/2}}{\beta V}, \quad (2)$$

which is used as a plot of $\ln(J/V^2)$ vs. $1/V$ (called the FN plot). In this study, the work function ϕ is interpreted as

$$\phi = V_{bi} - V_c, \quad (3)$$

where V_c is the cathode potential applied to the electric double layer. The anode potential was ignored because the anode impedance was 27 times smaller than that of the cathode. The impedance between the anode and cathode was also ignored because of the high solution content. Hence, the cathode potential is obtained by the following equation: $V_c = \text{the amplitude of the rectangular pulse voltage} - \text{the voltage drop across the } 22 \Omega \text{ resistor}$. The i element content C_i of an electrodeposit is given as

$$C_i \propto S_i J_i, \quad (4)$$

where S_i is the activity of element- i in the solution and J_i is the current that flows when the i -element changes from an ion to an atom according to Eq. (1).

When the cathode potential is equal to the potential barrier, electrons transfer to one of the multiple quantized rotational energy levels as shown Fig. 2 (b). As reported in [9], the transition is observed as the oscillation of the elemental content of the electrodeposited thin films at the resonant frequency.

When the cathode potential is greater than the potential barrier, electrons easily transfer to the upper state. The electric double layer acts as an impedance. Hence, the elemental content of the electrodeposited thin film is given by

$$C_i \propto S_i. \quad (5)$$

The i -element content is independent of the cathode potential.

In this study, the relationship between the cathode potential and the elemental content was investigated according to Eqs. (4) and (5).

3.2 Change in the elemental content for the applied cathode potential

3.2.1 Cathode potentials of 0.37 and 0.78 V

Figure 3 shows the dependence of the elemental content on the frequencies at cathode potentials of 0.37 and 0.78 V. The Co content was the highest among the elements of the Co–Ni–Fe–Mn thin films and slightly decreased with the cathode potential. In addition, the Co content was three times higher than the Ni content, whereas the Co^{2+} ion content in the solution was 2.7 times lower than the Ni^{2+} ion content.

The standard electrode potentials of Co^{2+} and Ni^{2+} are -0.282 and -0.236 V, respectively [10], which reveal no causal relationship with the Co and Ni contents. The Ni content was slightly lower than the Fe content, whereas the Ni^{2+} ion in the solution was 6 times higher than the Fe^{2+} ion content. The mean Mn content, which was an average taken over the frequency range of 0.4–1.2 MHz, was approximately 0.5 at % and substantially lower than that of the other elements.

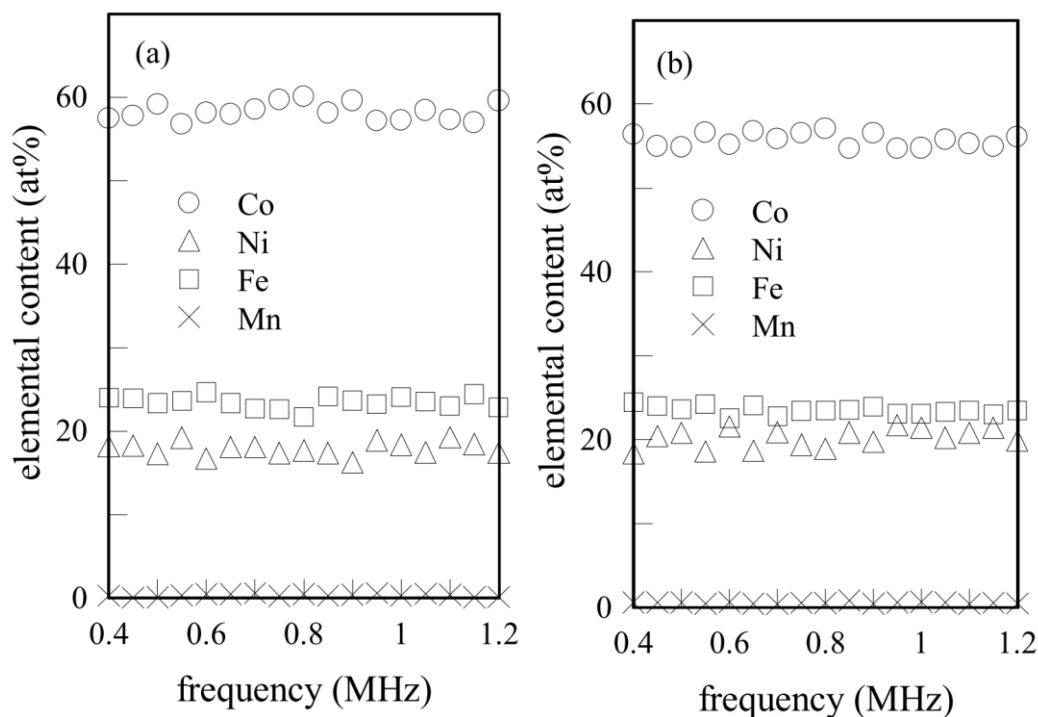


Figure 3. Plot of the elemental content of the Co–Ni–Fe–Mn thin films vs. the frequency: (a) $V_c = 0.37$ and (b) $V_c = 0.78$ V.

The BV equations for the elements cannot explain that all the element contents only slightly changed independent of a 2.1-fold increase in the cathode potential.

3.2.2 Cathode potential of 1.12 V

Figure 4 shows the dependence of the elemental content of Co–Ni–Fe–Mn thin films on the frequency. All the elements showed the oscillatory behaviors at resonant frequencies. This oscillation is explained in Fig.2 (b), that is, when the cathode potential is equal to the potential barrier of an element, the oscillation of the element content occurs owing to the electron transition to the quantized rotational energy levels at the resonant frequencies [9].

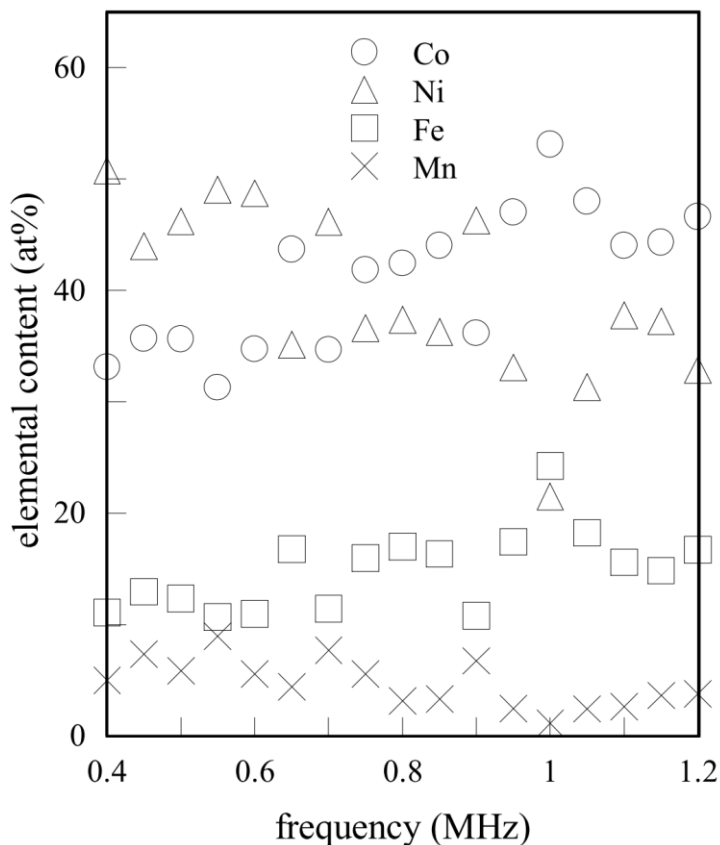


Figure 4. Plot of the elemental content of the Co–Ni–Fe–Mn thin films vs. the frequency at $V_c = 1.12$.

In Section 3.3, the element that caused the oscillation was identified. Compared to Fig. 3, the Ni and Mn content increased, whereas the Co and Fe content decreased. The mean Co and Ni contents, which were 40.6 and 39.8 at%, respectively, exhibited only a slight difference. The content of Mn was 4.7 at%, which was 10 times higher than the content of Mn electrodeposited at cathode potentials of 0.37–0.78 V.

3.2.3 Cathode potentials of 1.48–4.93 V

Figure 5 shows the dependence of the elemental content on the frequency. The content of the four elements of the Co–Ni–Fe–Mn thin films changed slightly with the cathode potentials. This is because the cathode potentials were larger than all the potential barriers shown in Fig.2 (c). The Ni content, which was the second highest content in Figs. 2 and 3, was the highest one. The contents of Co^{2+} , Ni^{2+} , Fe^{2+} , and Mn^{2+} in the solution were 21.7, 58.7, 9.78, and 9.78 at %, respectively. The mean contents of Co, Ni, Fe, and Mn of the Co–Ni–Fe–Mn thin films were 28.2, 53.2, 10.0, and 8.8 at %, respectively. The differences in the four element contents between the Co–Ni–Fe–Mn thin films and the solution were small. The elemental content of the Co–Ni–Fe–Mn thin films corresponds to the effective concentrations, that is, the activity of S_i .

3.3. Elemental content normalized by Fe content

As shown in Figs. 3, 4 and 5, the elemental content of the Co–Ni–Fe–Mn thin films seems to change intricately with the cathode potential. In Table 1, the mean elemental content of the Co–Ni–Fe–Mn thin films is summarized. A change in the content of one element causes changes in the other element contents because the summation of the contents should be 100 at%. Hence, the change in the elemental content with the cathode potential appears complex. According to Eq. (5), the elemental content has a constant value when the cathode potential is larger than its potential barrier. Hence, the elemental content normalized by the element with a constant content confirms the dependence of the contents on the cathode potential.

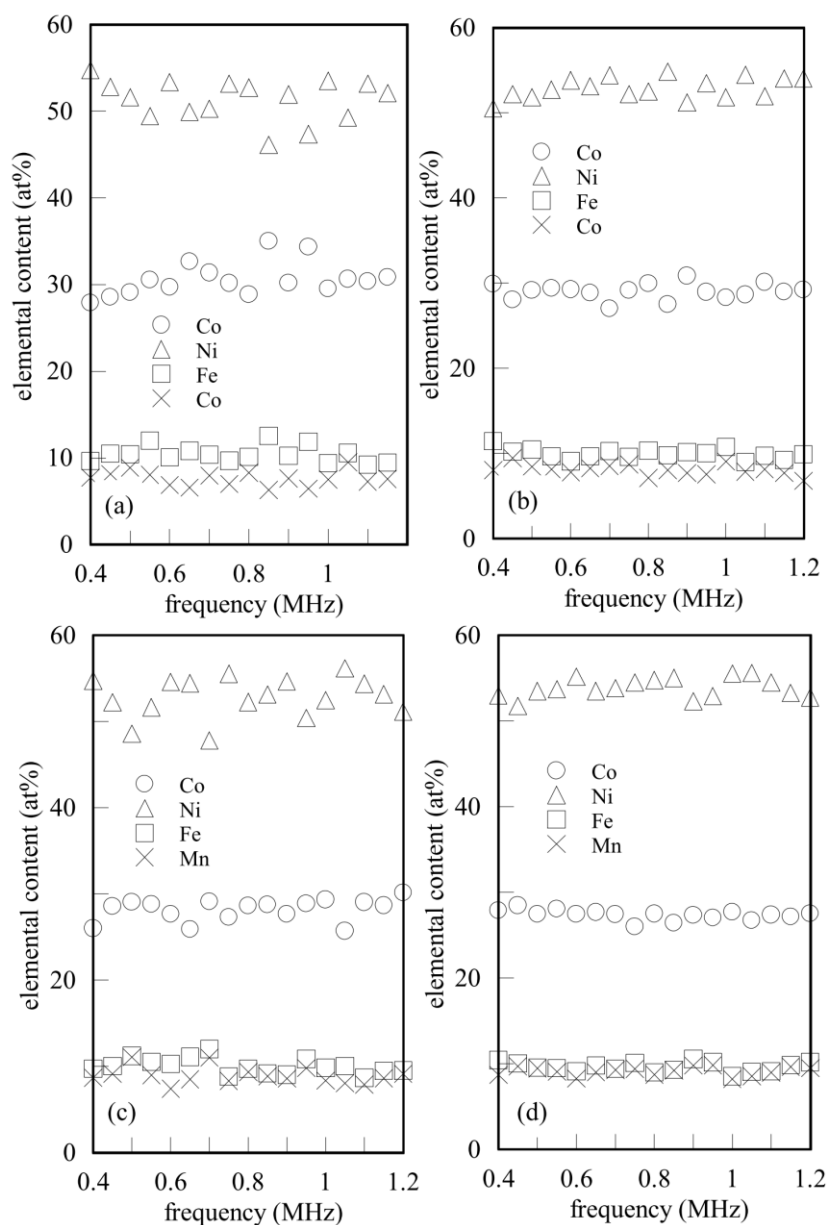


Figure 5. Plot of the elemental content of the Co–Ni–Fe–Mn thin films vs. frequency: (a) $V_c = 1.48$, (b) $V_c = 2.3$, (c) $V_c = 3.12$, and (d) $V_c = 4.93$ V.

Table 1. Mean elemental content (at%) of the Co–Ni–Fe–Mn thin films in Figs. 3,4, and 5.

V _c (V) \ element	0.37	0.78	1.12	1.48	2.3	3.12	4.93
Co	58.3	55.7	40.6	30.6	29.1	28.2	27.4
Ni	17.9	20.2	39.8	51.4	52.9	52.8	53.9
Fe	23.5	23.5	14.8	10.4	10.0	10.0	9.6
Mn	0.33	0.57	4.7	7.6	8.1	8.9	9.1

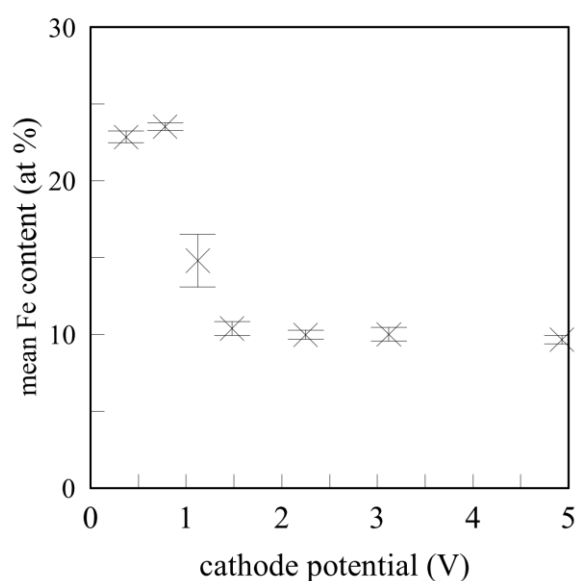
**Figure 6.** Cathode potential dependence of the mean Fe content of the Co–Ni–Fe–Mn thin films.

Figure 6 shows the dependence of the mean Fe content on the cathode potential. For the cathode potentials larger than 1.48 V, the mean Fe content exhibited a constant value. This indicates that all potential barriers were smaller than the cathode potentials. The mean Fe content increased when the cathode potentials changed from 0.78 to 1.12 V. The apparent increase in the mean Fe content was caused by decreases in the other element contents that have larger potential barriers than the cathode potentials. The mean Fe content slightly decreased at the cathode potential of 0.37 V compared to a cathode potential of 0.78 V. This was because the cathode potential was smaller than the Fe potential barrier. Hence, the Fe potential barrier is expected to exist in a range of 0.37–0.78 V. Thus, in this study, the mean Fe content was chosen as the normalization factor.

Figure 7 shows a plot of M_i/M_{Fe} vs. the cathode potential where M_i is the mean content of element $-i$. As shown in Fig. 6, the dependence of the element content on the cathode potential is revealed by the

normalization. The values of M_i/M_{Fe} ($i = \text{Co, Ni, and Mn}$) increase with cathode potentials larger than 0.78 V and attain constants. However, at the cathode potential of 0.37 V, each elemental content exhibits different behaviors because M_{Fe} has a smaller value than that at 0.78 V, as explained in Fig. 6.

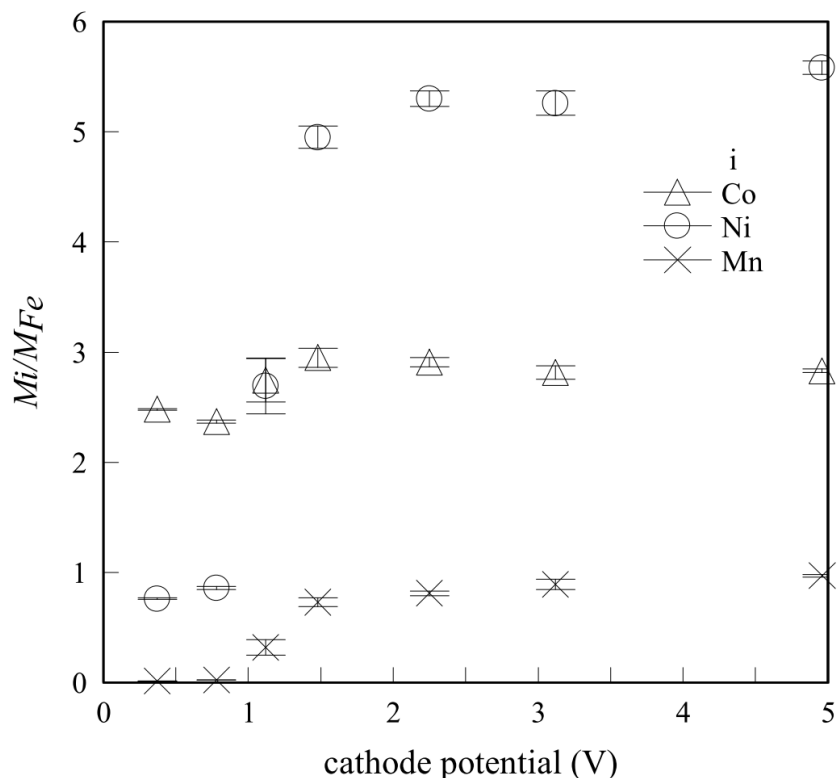


Figure 7. Plot of the mean elemental content normalized by the mean Fe content vs. cathode potential.

An increase in M_i/M_{Fe} with the cathode potential indicates that each potential barrier of the element is larger than the cathode potential and M_i/M_{Fe} is expected to obey the Fowler-Nordheim equation.

At the cathode potential of 1.12 V, M_{Co}/M_{Fe} exhibits a large variance owing to the oscillation as shown in Fig. 6, and deviates only slightly from its fixed value. Hence, the potential value of 1.12 V is consistent with the potential barrier of Co^{2+} . The potential barriers are defined as the points of the intersection of the straight line that has a constant M_i/M_{Fe} and the line with the slope of M_i/M_{Fe} . The potential barriers obtained from Fig. 7 are listed in Table 2. Using the definition of the potential barrier in this study, the potential barriers of Ni^{2+} and Mn^{2+} were larger than 1.48 V.

Table 2. Potential barriers of Co^{2+} , Ni^{2+} , Fe^{2+} , and Mn^{2+} obtained from Fig. 7.

element	Co^{2+}	Ni^{2+}	Fe^{2+}	Mn^{2+}
potential barrier (V)	1.12	1.56	Between 0.37 and 0.78	1.67

The constant values of M_i/M_{Fe} for cathode potentials > 2 V indicate that the system was not in a diffusion-limited state [3], but each potential barrier of the element was smaller than the cathode potential.

Figure 8 shows the FN plot of Ni^{2+} and Mn^{2+} for the cathode potential of 0.78–1.48 V using the potential barrier in Table 2. The values lie on a straight line, as expected in Eq. (2). The slopes of the two straight lines that are equal to α/β in Eq. (2) yield the values of β for Ni^{2+} and Mn^{2+} , 1.21×10^8 and $0.313 \times 10^8 \text{ cm}^{-1}$, respectively. The values of β are reasonable because the thickness of the electric double layer is of the order of $1 \times 10^{-8} \text{ cm}$.

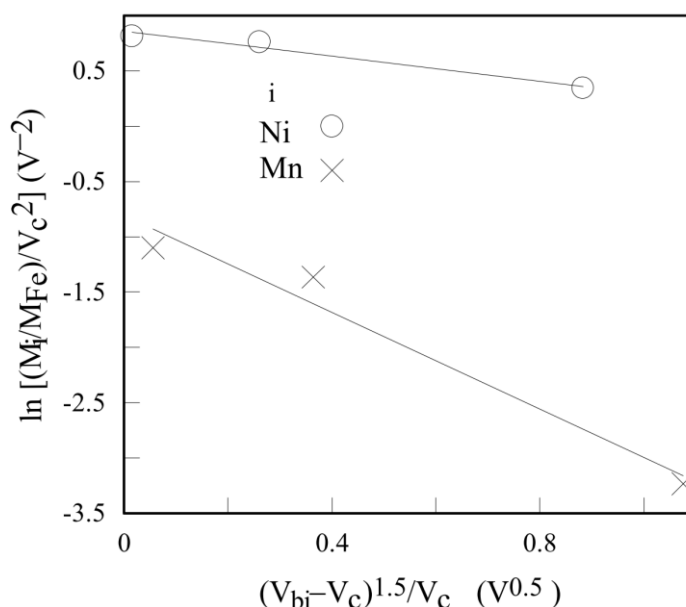


Figure 8. Fowler-Nordheim plot of the mean Ni and Mn contents.

4. CONCLUSIONS

Using the energy band diagram proposed in this study, the mean elemental content of the Co–Ni–Fe–Mn thin films was demonstrated by the relationship between the cathode potential V_c and potential barrier V_{bi} of the i -element: for $V_{bi} < V_c$, the i -element content of the Co–Ni–Fe–Mn thin film was consistent with the activity of the i -element in the solution, for $V_{bi} = V_c$, the i -element content showed oscillation, and for $V_{bi} > V_c$, the element contents obeyed the FN equation. Hence, the elemental content of multi-element electrodeposits can be predicted by the cathode potential and potential barriers of the elements.

References

1. J. D. Costa, M. B. de Sousa, J. J. N. Alves, B. de O. Evaristo, R. A. Queiroga, A. X. dos Santos, T. M. Maciel, A. R. N. Campos, R. A. C. de Santana, and S. Prasad, *Int. J. Electrochem. Sci.*, 13

- (2018) 2969.
2. Yijia Zhang & Patrick J. Shamberger, *Sci. Rep.*, 8 (2018) 1.
 3. R. K. Pandey, S. N. Sahu, and S. Chandra, *Handbook of Semiconductor Electrodeposition* (1996), Marcel Dekker, New York, USA.
 4. G. Grosso and G. P. Parravicini, *Solid State Physics* (2003), Academic Press, San Diego, USA.
 5. R. H. Fowler and L. Nordheim, *Proc. R. Soc. Ser. A*, 119 (1928) 173.
 6. M. Zubair, Y. S. Ang, and L. K. Ang, *IEEE Trans. Electron Devices*, 65 (2018) 2089.
 7. K. L. Jensen, *J. Appl. Phys.*, 126 (2019) 065302.
 8. M. Saitou, K. Hamaguchi and K. Inoue, *J. Phys. Chem. B*, 106 (2002) 12253.
 9. M. Saitou, *Int. J. Electrochem. Sci.*, 13 (2018) 305.
 10. D. R. Lide, *CRC Handbook of Chemistry and Physics*, CRC Press (1998), New York, USA.

© 2020 The Authors. Published by ESG (www.electrochemsci.org). This article is an open access article distributed under the terms and conditions of the Creative Commons Attribution license (<http://creativecommons.org/licenses/by/4.0/>).